Erschienen in: Advanced Materials ; 31 (2019), 17. - 1807521
https://dx.doi.org/10.1002/adma.201807521

Self-Assembling Proteins as High-Performance Substrates for Embryonic Stem Cell Self-Renewal

Christopher J. Hill, Jennifer R. Fleming, Masoumeh Mousavinejad, Rachael Nicholson, Svetomir B. Tzokov, Per A. Bullough, Julius Bogomolovas, Mark R. Morgan, Olga Mayans, and Patricia Murray**

The development of extracellular matrix mimetics that imitate niche stem cell microenvironments and support cell growth for technological applications is intensely pursued. Specifically, mimetics are sought that can enact control over the self-renewal and directed differentiation of human pluripotent stem cells (hPSCs) for clinical use. Despite considerable progress in the field, a major impediment to the clinical translation of hPSCs is the difficulty and high cost of large-scale cell production under xeno-free culture conditions using current matrices. Here, a bioactive, recombinant, protein-based polymer, termed ZT^{Fn}, is presented that closely mimics human plasma fibronectin and serves as an economical, xeno-free, biodegradable, and functionally adaptable cell substrate. The ZT^{Fn} substrate supports with high performance the propagation and long-term self-renewal of human embryonic stem cells while preserving their pluripotency. The ZT^{Fn} polymer can, therefore, be proposed as an efficient and affordable replacement for fibronectin in clinical grade cell culturing. Further, it can be postulated that the ZT polymer has significant engineering potential for further orthogonal functionalization in complex cell applications.

The generation of substrates that preserve pluripotency in human stem cells and direct their controlled differentiation is intensely pursued.[1,2] Such substrates are of critical value to stem-cell-based applications, such as those concerning the modeling of disease, drug discovery, the screening of toxicants, and personalized therapies in regenerative medicine for conditions like age-related macular degeneration and Parkinson's disease.[3,4] Human pluripotent stem cells (hPSCs), specifically human embryonic stem cells (hESCs) and induced pluripotent stem cells (iPSCs), are of critical significance in these pursuits.[5] Biomedical applications of hPSCs require large-scale ex vivo culture. Therapeutic uses require, in addition, xeno-free conditions to avoid risk of zoonotic transmission. Meeting these combined requirements is challenging as hPSCs are typically cultured on costly animal-derived substrates of undefined and variable batch-to-batch composition. In particular, hPSCs are commonly cocultured with mouse fibroblast feeder cells or grown on Matrigel, a complex mixture of extracellular matrix (ECM) proteins secreted by mouse sarcoma cells that consists primarily of laminin, collagen IV, and entactin.[6] Recently, substrates based on the recombinant eukaryotic expression of ECM proteins such as laminin or vitronectin have been introduced.[7,8] These successfully support hPSC self-renewal,[9,10]

Dr. C. J. Hill, M. Mousavinejad, R. Nicholson, Dr. M. R. Morgan, Prof. P. Murray
Department of Cellular and Molecular Physiology
Institute of Translational Medicine
University of Liverpool
Nuffield Building, Crown Street, Liverpool L69 3BX, UK
E-mail: P.A.Murray@liverpool.ac.uk

Dr. C. J. Hill, Prof. O. Mayans
Department of Biochemistry
Institute of Integrative Biology
University of Liverpool
Crown Street, Liverpool L69 7ZB, UK
E-mail: Olga.Mayans@uni-konstanz.de

Dr. J. R. Fleming, Prof. O. Mayans
Department of Biology
University of Konstanz
78457 Konstanz, Germany

Dr. S. B. Tzokov, Prof. P. A. Bullough
Department of Molecular Biology and Biotechnology
The Krebs Institute
University of Sheffield
Sheffield S10 2TN, UK

Dr. J. Bogomolovas
Department of Medicine
UCSD
La Jolla, CA 92093, USA

Dr. J. Bogomolovas
Department of Cognitive and Clinical Neuroscience
Central Institute of Mental Health
Medical Faculty Mannheim
Heidelberg University
68159 Mannheim, Germany

but have high purchase costs. Together with the expense of clinical grade culture media, this limits the upscaling of hPSC expansion (e.g., in large-scale 3D culture systems using microcarriers[11]) using these substrates. Chemical substrates carrying conjugated peptides are also available, like Synthemax. However, in addition to their high cost, their use in therapeutic applications might raise potential safety concerns. For example, Synthemax is made of carboxylic acid-carrying acrylate, to which peptides derived from vitronectin are attached using chemical crosslinking.[12] It successfully supports hPSC expansion[12] but it has been observed to lead to genetic abnormalities in long-term cell cultures.[13] In summary, the need for economic and safe translational materials persists.

The protein polymer ZT[14] holds promise to meet the need for an economical, homogeneous, and functionally adaptable cell substrate of controlled composition. ZT exploits the complexation of the protein telethonin (Tel) with the two N-terminal immunoglobulin (Ig) domains from titin, Z1Z2, which occurs naturally in human sarcomeres. Tel is "sandwiched" between two antiparallel Z1Z2 doublets, forming a robust intermolecular β-sheet that spans the three components[15] (**Figure 1**A). Both Tel and Z1Z2 can be overexpressed recombinantly in bacteria with a high yield. The ZT polymer is based on a Z1Z2–Z1Z2 fusion tandem (Z_{1212}) that causes the spontaneous propagative assembly of Z1Z2:Tel complexes.[14] ZT components can be readily functionalized by genetically encoding functional moieties into the building blocks prior to their assembly. This strategy affords exact control on the position and stoichiometry of exogenous elements in the polymer. As proof of principle, ZT was engineered to display an affinity motif N-terminal to Tel that recruited gold nanoparticles to the polymer with nanoscale periodicity.[14] Moreover, the isolated Z1 domain showed that its CD loop permits the grafting of lengthy peptide motifs without causing fold perturbations, serving as an accessible and functional epitope.[16] Thereby, the ZT polymer can allow the incorporation of functional moieties in a controllable fashion.

Here, we aimed to exploit the polymeric nature, scaffolding capabilities, and ease of production of the ZT polymer to develop an economic substrate for culturing hESCs. Specifically, we aimed to mimic the efficiency of human fibronectin in supporting hESC self-renewal in serum-free conditions.[17,18] In fibronectin, the small peptide RGD in domain Fn10 is the critical integrin-binding motif mediating cell adhesion, spreading, and migration.[19] Accordingly, RGD peptide mimetics are frequently employed as adhesive moieties on substrates for cell culture applications.[20,21] hESCs do not attach to RGD peptides,[18] but a proteolytic 120 kDa fibronectin fragment containing the complete Fn10 domain successfully supported their self-renewal.[18] Building on this knowledge and on the fact that fibronectin supports cell attachment with higher efficacy than RGD alone,[22] we have assessed the mimetic potential of the ZT polymer functionalized with RGD and Fn10 moieties.

First, we established that the ZT polymer remains unaltered upon display of exogenous bioreactive motifs. For this, we created two functionalized Z_{1212} variants by genetically fusing DNA sequences: 1) a Z_{1212} tandem carrying the fibronectin GRGDS motif in the CD loop of the second Z1 domain (Z_{1212}^{RGD}) (Figure 1A,B) and 2) a Z_{1212} chimera where the Fn10 domain from fibronectin had been fused C-terminally to the tandem (Z_{1212}^{Fn}) via the same GETTQ linker sequence originally used to join Z1Z2 doublets[14] (Figure 1C). In Z_{1212}^{RGD}, the GRGDS sequence has higher affinity for integrins than the core RGD motif alone, with the flanking residues known to enhance cell attachment.[23,24] This resulted ultimately in the substitution of four native Z1 residues for a seven-residue peptide (Figure 1B). For comparison, a biologically inactive RGE version[22] was created (Z_{1212}^{RGE}).

The variants Z_{1212}^{RGD}, Z_{1212}^{RGE}, and Z_{1212}^{Fn} proved undemanding to produce recombinantly in *Escherichia coli* cultures. Pure, stable, and monodisperse samples of all variants were produced in high yields equivalent to the wild type protein Z_{1212} (>40 mg L^{-1} culture) (Figure S1A,B, Supporting Information). To test the capability of the variants to self-assemble, and given that the Z1Z2/Tel complex is the fundamental assembly unit of the ZT polymer, we considered that complexation of Tel by modified Z1Z2 samples at the native 2:1 ratio was evidence of undisrupted assembly in these variants. Therefore, we produced $Z1Z2^{RGD}$/Tel and $Z1Z2^{Fn}$/Tel complexes by in cellulo co-expression, studied their migration in size exclusion chromatography (SEC), and measured their molecular mass by SEC-coupled multi-angle laser light scattering (MALLS), confirming the expected 2:1 association (Figure S1C–E, Supporting Information). Next, we mixed the polymerizing Z_{1212} variants (Z_{1212}^{RGD}, Z_{1212}^{RGE}, and Z_{1212}^{Fn}) with Tel and confirmed assembly by native-PAGE (Figure S1F,G, Supporting Information) and electron microscopy (Figure 1D); the resulting polymers are here denoted as ZT^{RGD}, ZT^{RGE}, and ZT^{Fn}, respectively. Taken together, these results proved that the Z_{1212} building block could be successfully functionalized in both internal (CD loop) and external (C-terminus) positions, maintaining its structural integrity and its polymerization capability.

The conformation of the RGD motif influences the selectivity and affinity of the integrin receptors it engages and, thereby, its efficiency in cell adhesion.[22,24–26] Thus, we studied whether the RGD motif inserted in Z1 resembles the motif in the native Fn10. In Fn10, the motif is located within the FG β-hairpin loop that resembles a distorted type II' β-turn with high intrinsic flexibility.[25,27] To confirm the degree of structural mimicry achieved by the loop engineered in Z1, we elucidated the crystal structure of Z_{1212}^{RGD} at 3.0 Å resolution (Table S1, Supporting Information). The structure confirmed that the fold of Z1 is not altered by the inserted sequence, with the structure closely matching that of wild-type Z1 (rmsd = 0.47 Å to Z1 in Protein Data Bank (PDB) entry 2A38[28]) (Figure 1E). The inserted SSGRGDSS sequence formed a loop protruding from the surface of Z1 as expected, in quasi β-turn conformation and with evident signs of flexibility (Figure S2, Supporting Information), thereby reproducing the features of the native motif in fibronectin. Comparison of crystal structures for modified Z1 and Fn10 (PDB IDs: 1FNA, 1FNF, and 4MMX) showed that the engineered RGD motif locally adopts a similar conformation (Figure 1F,G). These data confirm the ability of the introduced sequence to emulate the native RGD motif.

We then tested whether the functionalized ZT polymer promoted spreading of murine mesenchymal stromal cells (mMSC) by comparing the relative efficiency of cell attachment to the ZT^{RGD} and ZT^{Fn} polymers. For this analysis, we employed the clonally-derived mMSC line D1, which tolerates a variety of RGD-based substrata.[29–31] We cultured mMSCs on nonadhesive

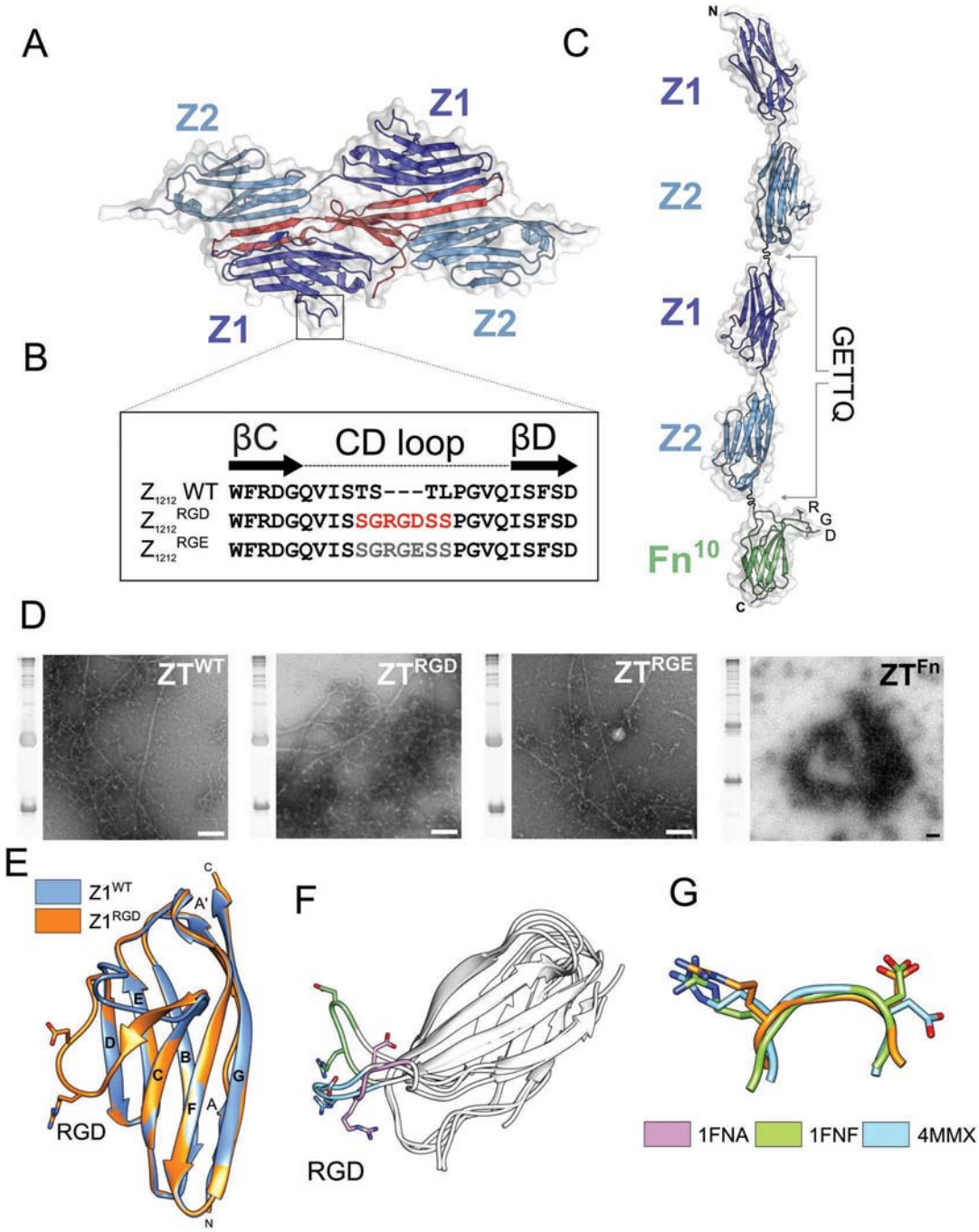

Figure 1. The functionalized ZT polymer. A) Crystal structure of the "sandwich" complex formed by two antiparallel Z1Z2 Ig-doublets from titin (blue) and Tel (red) (PDB: 1YA5[15]). The CD loop of domain Z1 is boxed. B) Sequence of the native and modified CD loop. The residues introduced are colored red. C) Z_{1212} protein carrying a C-terminally fused domain Fn10 from human fibronectin (PDB: 1FNF,[25] green). Fusion of naturally-occurring protein moieties in this chimera uses a GETTQ linker sequence. The native RGD motif located within the FG loop of Fn10 is displayed. D) Transmission electron microscopy images of ZT^{WT}, ZT^{RGD}, ZT^{RGE}, and ZT^{Fn} polymers postassembly (scale bars correspond to 100 nm). E) Crystal structure of the GRGDS modified Z1 domain superimposed on wild-type Z1 (PDB 2A38[28]). F) Superimposition of crystal structures of domain Fn10 from fibronectin (PDB codes are given). The conformational flexibility of the RGD loop (colored) is manifest. G) Superimposition of the RGD loop in Z1 (orange) with those from Fn10 structures shows that the motif incorporated in Z1 adopts a near-native conformation at the local level (structure 1FNA is excluded as its conformation is unique).

polystyrene plates coated with the ZT^{RGD}, ZT^{RGE}, and ZT^{Fn} polymers under serum-free conditions and quantified cell attachment and dispersion. At 2 h culture, mMSCs showed adherence to both ZT^{RGD} and ZT^{Fn} in a concentration-dependent manner, confirming the accessibility of both RGD and Fn10 moieties within the polymer (**Figure 2**A,B). However, consistently more

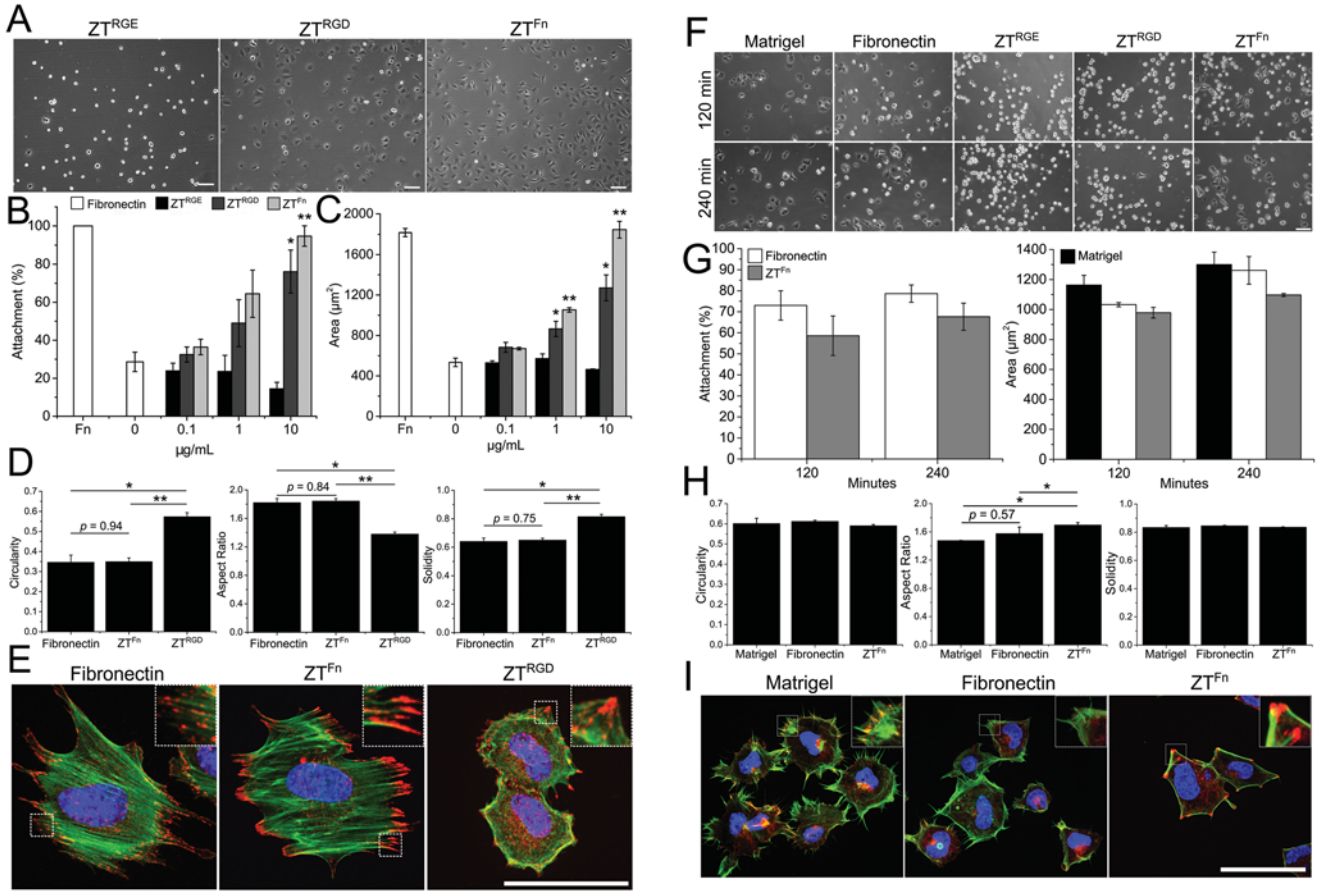

Figure 2. Murine MSC and human ESC adhesion and spreading on ZT substrates. A) Representative phase-contrast micrographs of mMSCs cultured for 2 h under serum-free conditions on nontreated plastic coated with ZT polymers at 10 μg mL^{-1} (scale bar = 100 μm). B,C) Effect of ZT^{RGE} (non-bioactive), ZT^{RGD}, and ZT^{Fn} substrates on mMSC adhesion (B) and spreading (C). Cell attachment is expressed as a percentage of the positive control (fibronectin at 10 μg mL^{-1}) that was taken as 100%. The average area of cells grown on fibronectin is included for comparison. Statistical significance in (B) and (C) is in reference to a nontreated surface (0 μg mL^{-1}). D) Comparisons of the average circularity, aspect ratio, and solidity of cells grown on nontreated plastic coated with fibronectin, ZT^{RGD}, or ZT^{Fn}, all samples at 10 μg mL^{-1}. E) Representative confocal microscopy images of cells stained for F-actin (green), paxillin (red), and DAPI (blue) following attachment to different substrates. Zooms of boxed areas are shown in the upper right of the respective image. F) Representative phase-contrast images of HUES7 cells cultured for 2 and 4 h on ZT^{RGD}, ZT^{Fn}, and control substrates. Scale bar = 100 μm. G) Quantification of cell attachment and spreading is shown by the bar charts. Cell attachment is expressed as a percentage of the positive control (Matrigel) that was taken as 100%. H) Comparisons of the average circularity, aspect ratio, and solidity of cells plated on plastic plates coated with Matrigel, fibronectin, or ZT^{Fn} at 10 μg mL^{-1}. I) Representative confocal microscopy images of cells stained for F-actin (green), paxillin (red), and DAPI (blue) following attachment to different substrates. Zooms of boxed areas are shown in the upper right of the respective image. (Error bars represent the standard error on the mean (SEM), $n = 3$. Scale bar = 50 μm if not otherwise stated. Throughout, $*p < 0.05$, $**p < 0.01$, and $***p < 0.001$).

cells attached to ZT^{Fn} than to ZT^{RGD}. As expected, the non-bioactive ZT^{RGE} did not support cell attachment. mMSC spreading was quantified by calculating the average cell area for all conditions (Figure 2C). Spreading was significantly increased on ZT^{RGD} and ZT^{Fn} compared to the plastic control, but ZT^{Fn} showed the best performance. In addition, cell profiles were used to determine the average circularity (or area-to-perimeter ratio), aspect ratio (AR), and solidity of mMSCs plated on human plasma fibronectin, ZT^{RGD} or ZT^{Fn} (Figure 2D). Values were remarkably equivalent for cells grown on ZT^{Fn} or fibronectin, while differences were observed in cells plated on ZT^{RGD}. Higher circularity and solidity values for mMSCs cultured on ZT^{RGD} correlated with a symmetric spreading on this substrate, while the higher AR and lower solidity of cells cultured on ZT^{Fn} or fibronectin indicate anisotropic spreading. By using a competitive inhibition assay that employed a linear GRGDS peptide, we confirmed that the observed effects on cell attachment are due to the respective specificities of the engineered ZT^{RGD} and ZT^{Fn} polymers for integrin binding (Figure S3, Supporting Information). To further investigate attachment, we examined the impact of the different substrates on cytoskeletal organization and adhesion complexes (Figure 2E). Focal complexes were observed on all substrates. However, mMSCs plated on fibronectin or ZT^{Fn} displayed well-developed stress fiber networks, while cells attached to ZT^{RGD} exhibited fewer stress fibers and a cortical actin distribution. Taken together, cell adhesion and spreading data indicated that the loop-grafted GRGDS motif was insufficient to support effective mMSC attachment, but that the interaction of cells with the ZT^{Fn} polymer mimicked that of full-length human fibronectin.

To assess the capability of ZT^{Fn} to support cell growth in potential clinical applications, we then tested this polymer on human HUES7 cells, proving that hESCs attach to and proliferate on ZT^{Fn}. HUES7 cells neither attach nor spread on materials functionalized with RGD peptides, but they can be cultured on fibronectin or large proteolytic fragments thereof.[18] Accordingly, we confirmed that HUES7 cells did not adhere to ZT^{RGD} (Figure 2F) or to the Fn10 domain alone (in the absence of the polymerized ZT) (Figure S4, Supporting Information). However, they attached successfully to the ZT^{Fn} polymer. Moreover, the extent of HUES7 cell attachment and spreading on ZT^{Fn} was comparable to that on human plasma fibronectin (both substrates used at comparable amounts; Figure S5, Supporting Information). Cell attachment and spreading on both fibronectin and ZT^{Fn} were only moderately lower than those obtained from the complex matrix Matrigel (Figure 2G). We concluded that the ZT^{Fn} polymer comparatively resembled the performance of native fibronectin in supporting hESC growth and spreading.

We further compared the effect of ZT^{Fn}, fibronectin, and Matrigel on cell growth. As our long-term goal is to support the clinical application of hPSCs, we focused this test on established biological substrates, naturally produced by living cells and composed only of biodegradable, folded protein components that have not undergone chemical treatment. We did not employ chemical substrates (e.g., Synthemax) as comparative controls to ZT^{Fn} because of their more distant composition. The results showed that, while average cell circularity and solidity were consistent between substrates, the average AR of cells plated on ZT^{Fn} was significantly higher than that of cells cultured on fibronectin and particularly higher than Matrigel, reflecting the asymmetric spreading on ZT^{Fn} (Figure 2H). F-actin and paxillin staining showed that focal adhesions were present in HUES7 cells grown on Matrigel and ZT^{Fn}, but were less common on fibronectin (Figure 2I). Filopodia-like projections were abundant in cells cultured on Matrigel and in some cells grown on fibronectin, but cells grown on ZT^{Fn} lacked projections and exhibited a geometric morphology with well-defined actin stress fibers (Figure 2I). Intriguingly, the observed increase in actin filamentation was sustained following prolonged culture on ZT^{Fn} (Figure S6A, Supporting Information). Despite their morphological differences, cells grown on ZT^{Fn} retained an ESC phenotype following single cell dissociation as confirmed by nuclear OCT4 and NANOG expression (Figure S6B, Supporting Information). Cells on all substrates successfully began to form colonies after 24 h (Movies S1–S3, Supporting Information) and robustly expressed pluripotency markers (Figure S7A, Supporting Information). Additionally, focal adhesions were found to contain focal adhesion kinase (FAK) phosphorylated at tyrosine 397 (pY397), confirming the activation of signaling pathways downstream of integrin engagement (Figure S7B, Supporting Information).

To better characterize the molecular mode of action of ZT^{Fn}, we set out to identify the integrins it engages. As fibronectin attachment is largely dependent on $\alpha5\beta1$ and $\alpha V\beta3$,[32] we tested first the involvement of these integrins in HUES7 cells plated on ZT^{Fn}. While we detected $\alpha5\beta1$ in focal adhesions (**Figure 3**A), we did not detect $\alpha V\beta3$ (Figure S8A,B, Supporting Information). Unexpectedly, targeting the αV subunit alone produced robust focal adhesion-like staining, as did an antibody against subunit $\beta5$ unique to the $\alpha V\beta5$ heterodimer (Figure 3B). Thus, we concluded that HUES7 cell attachment to ZT^{Fn} is mediated by $\alpha V\beta5$ and $\alpha5\beta1$ integrins present in cell adhesion complexes (Figure 3C). After 2 days of culture, the cells continued to engage $\alpha V\beta5$ (Figure S9, Supporting Information). On the contrary, cells grown on Matrigel and fibronectin were negative for both αV and $\beta5$ adhesion-specific staining (Figure S8B, Supporting Information). Currently, there is no robust evidence for the binding of $\alpha V\beta5$ to fibronectin; therefore, its engagement by ZT^{Fn} was unexpected. Integrin $\alpha V\beta5$ is a well-characterized receptor of the RGD motif in the somatomedin-B domain from vitronectin.[33,34] Accordingly, $\alpha V\beta5$ mediates hPSC attachment to vitronectin,[35,36] and attachment of hiPSC lines IMR90 and Gibco episomal line to the synthetic vitronectin-based peptide acrylate, Synthemax.[12] In agreement with our finding, we observed that the morphology of cells grown on ZT^{Fn} strikingly emulated that of cells grown on vitronectin (Figure S10, Supporting Information). Both cells cultured on vitronectin and ZT^{Fn} also displayed increased stress fiber formation and large focal adhesions containing FAK pY397 (Figure S10, Supporting Information). The larger size of focal adhesions formed on the ZT^{Fn} substrate caused the cells to migrate more slowly in comparison to Matrigel and fibronectin substrates, as a close relationship exists between the size of focal adhesions and cell migration speed (Figure 3D).[37] Slow migration was reproduced by cells cultured on vitronectin (Figure 3D). Upon prolonged culture on all substrates, cells formed colonies. Colonies grown on Matrigel exhibited $\alpha5\beta1$ expression in distinct fibrillar patterns while expression of this integrin was lost on ZT^{Fn} (Figure S9A, Supporting Information). Yet, colonies grown on ZT^{Fn} continued to express $\alpha V\beta5$ (Figure S9B, Supporting Information). It is remarkable to observe that the presentation of the Fn10 domain in the context of the ZT^{Fn} polymer induces a preferential switch to $\alpha V\beta5$. It can be concluded that not only the chemical composition of the bioreactive motif but also the geometry of its presentation to the cell is critical for integrin selectivity. This finding adds to the previous observation that the specific conformation of fibronectin on different synthetic surfaces dramatically influenced integrin binding.[38]

To investigate whether the observed difference in integrin engagement affected cell phenotype, we assessed the ability of ZT^{Fn} to promote survival of single HUES7 cells. We found that hESCs maintain a pluripotent phenotype following prolonged culture on ZT^{Fn}, which supported clonal expansion with an efficacy comparable to fibronectin and only moderately reduced relative to Matrigel (**Figure 4**A). Cell proliferation was somewhat reduced on ZT^{Fn} compared to Matrigel, but was not significantly different from fibronectin (Figure 4B). Finally, we assessed the ability of ZT^{Fn} to maintain the long-term self-renewal of HUES7 cells. For this, the cells were cultured in mTeSR1 medium (without ROCK inhibitor, a compound used to extend cell survival[39]) for up to 18 passages. The cells were passaged every 5–6 days as clumps containing 50–200 cells; they were cultured on ZT^{Fn} for ≈4 months in total with no noticeable negative effects. The cells grew as colonies with typical morphologies, including a high nuclear-to-cytoplasmic ratio and prominent nucleoli. Cells also retained nuclear expression of OCT4 and NANOG (Figure S11A, Supporting Information). Relative gene expression analysis of pluripotency markers OCT4, NANOG, and SOX2 was used to compare cells cultured on Matrigel with those cultured on fibronectin or ZT^{Fn} for 1, 5, and

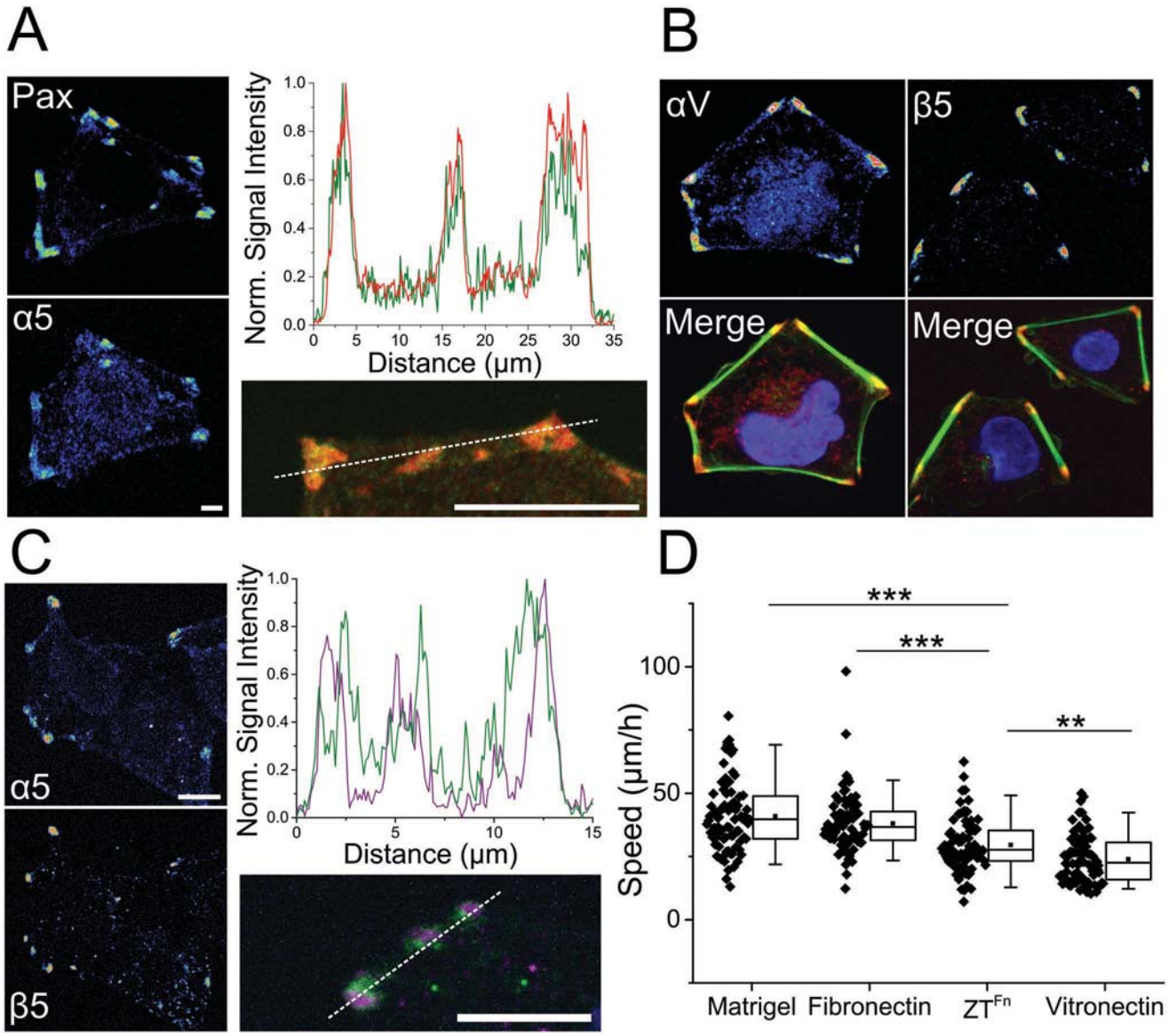

Figure 3. Integrin engagement and migration of human ESCs on ZT^{Fn}. A) Representative pseudocolored confocal microscopy images show paxillin (red) and α5 integrin subunit (green) costaining of HUES7 cells following 4 h culture on ZT^{Fn}. The fluorescence intensity line scan profile was generated from the merged image shown below. Scale bars = 10 μm. B) Staining of αV and β5 integrin subunits (red). The merged images show counterstaining for F-actin (green) and DAPI (blue). Scale bar = 50 μm. C) Pseudocolored microscopy images show costaining of α5 (green) and β5 (purple) subunits in HUES7 cells cultured on ZT^{Fn}. A fluorescence intensity profile is shown for the merged image. Scale bars = 10 μm. D) Box-and-whisker plots of cell migration. Boxes show the median (middle line), mean (square), 25th and 75th percentiles (box ends), and 5th and 95th percentiles (whiskers) ($n = 80$).

10 passages. *NANOG* and *SOX2* transcript levels were found to be significantly decreased in cells cultured on fibronectin at passage 10 (Figure 4C). Although NANOG expression was also downregulated in cells cultured on ZT^{Fn} at passage 10 relative to Matrigel, expression was significantly higher compared to fibronectin (Figure 4C). Cells cultured on ZT^{Fn} or fibronectin for 13 passages were used to form embryoid bodies that contained derivatives of the three embryonic germ layers in vitro (Figure S11B in Supporting Information). Positive staining for Brachyury (mesoderm), GATA6 (GATA-binding factor 6, endoderm), and Nestin (ectoderm) confirmed that HUES7 cells remained pluripotent following their long-term culture on ZT^{Fn}.

In conclusion, we show that the ZT polymer is a chimeric composite of recombinant human proteins, with high functionalization capability.[14] Neither loop grafting nor domain fusion reduced the bacterial production yield of Z_{1212} variants, an important consideration for large-scale applications. We show that the functionalized ZT system is compatible with standard cell culture techniques and that it serves as an efficient substrate for the long-term self-renewal of pluripotent hESCs, being a viable substitute for natural fibronectin and other commonly used matrices for hPSC culture. The material is produced in bacteria; it is scalable and predictably compatible with 3D culture systems. In this regard, the incorporation of natural ECM proteins with 3D

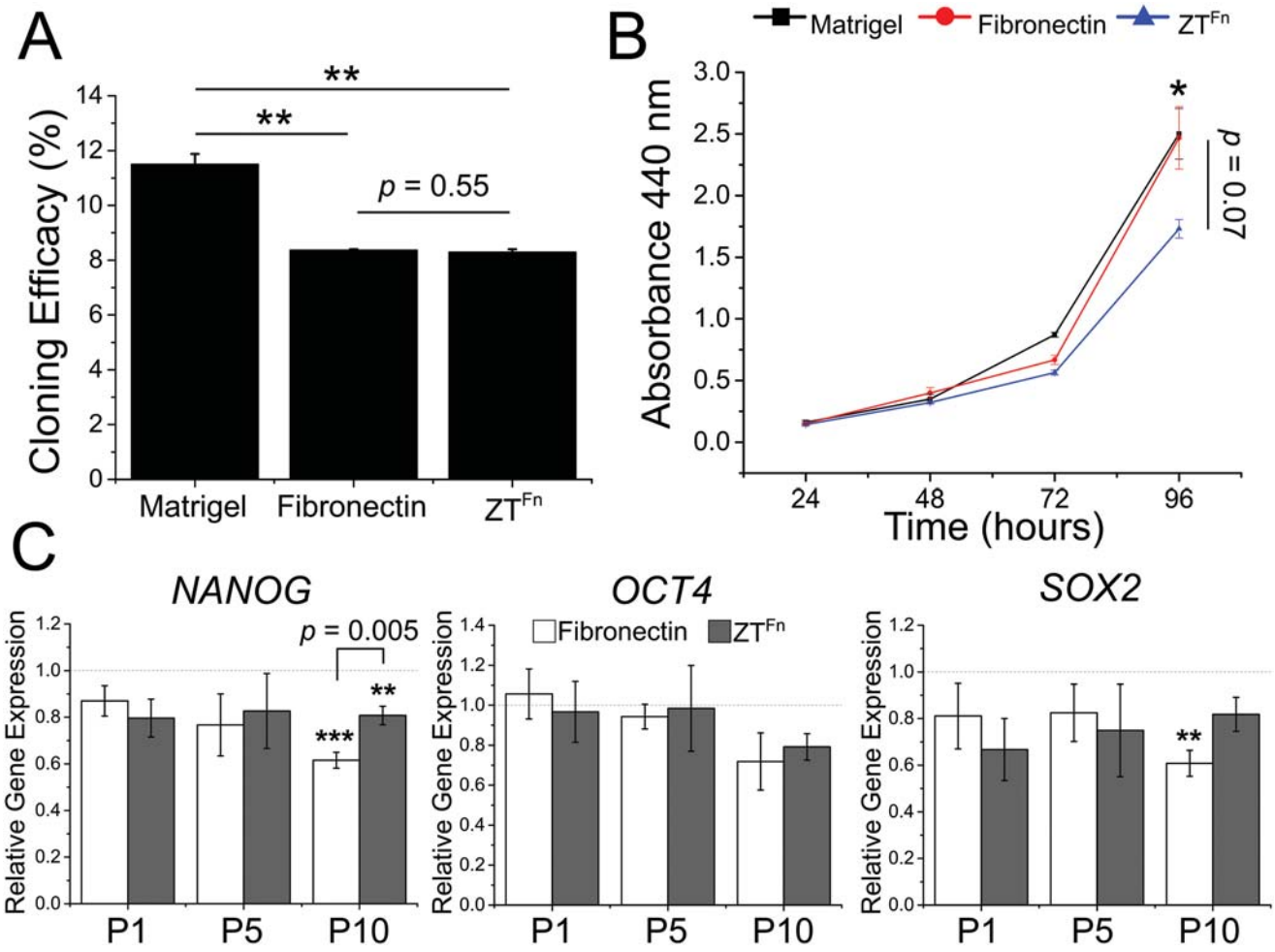

Figure 4. Human ESC clonal culturing and self-renewal on ZT^{Fn}. A) Clonogenic survival of cells plated on Matrigel, fibronectin, and ZT^{Fn} at a density of 2.5×10^3 cm^{-2}. B) Proliferative capacity of HUES7 cells cultured on Matrigel, fibronectin, or ZT^{Fn} over 4 days. Error bars represent SEM ($n = 4$). C) Quantitative RT-qPCR analysis of NANOG, OCT4, and SOX2 expression levels in HUES7 cells cultured on fibronectin or ZT^{Fn} for 1, 5, and 10 passages relative to cells cultured on Matrigel. Error bars represent SEM ($n = 3$).

materials using crosslinking is established in the bibliography. For example, fibronectin has been photocrosslinked into hyaluronic acid 3D hydrogels for endothelial cell culture.[40] As the ZT polymer is composed of folded protein domains that closely resemble those of fibronectin, its incorporation in 3D systems via chemical crosslinking can be expected to be an equally feasible goal. In summary, economical substrates of controlled composition such as the ZT^{Fn} polymer will be essential for further advancement in the clinical translation of PSC-based therapies.

Acknowledgements

The authors thank Yevheniia Nesterenko and the Electron Microscopy Unit of Universität Konstanz for EM images of ZT^{Fn}. The authors thank the Diamond Light Source for synchrotron radiation time. This research was supported by the BBSRC (Biotechnology and Biological Sciences Research Council), JRI Orthopaedics (BB/I01666X/1), and the Wellcome Trust (204401/z/16/z). J.R.F. was supported by an EU Marie Sklodowska-Curie Individual Fellowship (TTNPred, 753054). The authors thank the HUES cells facility, Melton Laboratory, Harvard University, MA (USA) for providing the HUES7 cell line. The mMSC cell line was purchased from ATCC. C.J.H., O.M., and P.M. conceived the study. C.J.H., O.M., M.R.M., and P.M. designed experiments. C.J.H. and J.B. performed molecular cloning. C.J.H produced and characterized protein constructs and assemblies. C.J.H., S.B.T., and P.A.B. carried out electron microscopy studies. C.J.H., J.R.F., and O.M. analyzed protein structure. C.J.H., M.M., and R.N. performed cell-based experiments and data analysis. C.J.H. performed confocal imaging. C.J.H., O.M., P.M., and M.R.M. wrote the manuscript. The coordinates and X-ray diffraction data for the crystal structure of $Z_{1212}{}^{RGD}$ have been deposited with the Protein Data Bank (www.rcsb.org) with accession code 6FWX.

Conflict of Interest

The authors declare competing financial interests: C.J.H., O.M., and P.M. disclose a pending patent on the use of Fn10 as a chimeric fusion protein of the ZT system.

Keywords

biomaterials, protein engineering, protein self-assembly, self-renewal, stem cells

[1] C. M. Madl, S. C. Heilshorn, *Annu. Rev. Biomed. Eng.* **2018**, *20*, 21.
[2] Z. Liu, M. Tang, J. Zhao, R. Chai, J. Kang, *Adv. Mater.* **2018**, *30*, 1705388.
[3] R. S. Thies, C. E. Murry, *Development* **2015**, *142*, 3614.
[4] Y. Avior, I. Sagi, N. Benvenisty, *Nat. Rev. Mol. Cell Biol.* **2016**, *17*, 170.
[5] Y. Shi, H. Inoue, J. C. Wu, S. Yamanaka, *Nat. Rev. Drug Discovery* **2017**, *16*, 115.
[6] C. S. Hughes, L. M. Postovit, G. A. Lajoie, *Proteomics* **2010**, *10*, 1886.
[7] E. Sanjar, S. Jin, *World J. Stem Cells* **2015**, *7*, 243.
[8] Y. Fan, J. Wu, P. Ashok, M. Hsiung, E. S. Tzanakakis, *Stem Cell Rev. Rep.* **2015**, *11*, 96.
[9] A. B. J. Prowse, M. R. Doran, J. J. Cooper-White, F. Chong, T. P. Munro, J. Fitzpatrick, T. L. Chung, D. N. Haylock, P. P. Gray, E. J. Wolvetang, *Biomaterials* **2010**, *31*, 8281.
[10] T. Miyazaki, S. Futaki, H. Suemori, Y. Taniguchi, M. Yamada, M. Kawasaki, M. Hayashi, H. Kumagai, N. Nakatsuji, K. Sekiguchi, E. Kawase, *Nat. Commun.* **2012**, *3*, 1236.
[11] C. Kropp, D. Massai, R. Zweigerdt, *Process Biochem.* **2017**, *59*, 244.
[12] Z. Melkoumian, J. L. Weber, D. M. Weber, A. G. Fadeev, Y. Zhou, P. Dolley-Sonneville, J. Yang, L. Qiu, C. A. Priest, C. Shogbon, A. W. Martin, J. Nelson, P. West, J. P. Beltzer, S. Pal, R. Brandenberger, *Nat. Biotechnol.* **2010**, *28*, 606.
[13] J. W. Lambshead, L. Meagher, J. Goodwin, T. Labonne, E. Ng, A. Elefanty, E. Stanley, C. M. O'Brien, A. L. Laslett, *Sci. Rep.* **2018**, *8*, 701.
[14] M. Bruning, L. Kreplak, S. Leopoldseder, S. A. Muller, P. Ringler, L. Duchesne, D. G. Fernig, A. Engel, Z. Ucurum-Fotiadis, O. Mayans, *Nano Lett.* **2010**, *10*, 4533.
[15] P. Zou, N. Pinotsis, S. Lange, Y.-H. Song, A. Popov, I. Mavridis, O. M. Mayans, M. Gautel, M. Wilmanns, *Nature* **2006**, *439*, 229.
[16] M. Bruning, I. Barsukov, B. Franke, S. Barbieri, M. Volk, S. Leopoldseder, Z. Ucurum, O. Mayans, *Protein Eng., Des. Sel.* **2012**, *25*, 205.
[17] M. A. Baxter, M. V. Camarasa, N. Bates, F. Small, P. Murray, D. Edgar, S. J. Kimber, *Stem Cell Res.* **2009**, *3*, 28.
[18] D. M. Kalaskar, J. E. Downes, P. Murray, D. H. Edgar, R. L. Williams, *J. R. Soc., Interface* **2013**, *10*, 20130139.
[19] A. J. Zollinger, M. L. Smith, *Matrix Biol.* **2017**, *60–61*, 27.
[20] L. Perlin, S. Macneil, S. Rimmer, *Soft Matter* **2008**, *4*, 2331.
[21] S. L. Bellis, *Biomaterials* **2011**, *32*, 4205.
[22] P. Rajagopalan, W. A. Marganski, X. Q. Brown, J. Y. Wong, *Biophys. J.* **2004**, *87*, 2818.
[23] M. D. Pierschbacher, E. Ruoslahti, *Nature* **1984**, *309*, 30.
[24] T. G. Kapp, F. Rechenmacher, S. Neubauer, O. V. Maltsev, E. A. Cavalcanti-Adam, R. Zarka, U. Reuning, J. Notni, H. J. Wester, C. Mas-Moruno, J. Spatz, B. Geiger, H. Kessler, *Sci. Rep.* **2017**, *7*, 39805.
[25] D. J. Leahy, I. Aukhil, H. P. Erickson, *Cell* **1996**, *84*, 155.
[26] E. Ruoslahti, B. Obrink, *Exp. Cell Res.* **1996**, *227*, 1.
[27] A. L. Main, T. S. Harvey, M. Baron, J. Boyd, I. D. Campbell, *Cell* **1992**, *71*, 671.
[28] M. Marino, P. Zou, D. Svergun, P. Garcia, C. Edlich, B. Simon, M. Wilmanns, C. Muhle-Goll, O. Mayans, *Structure* **2006**, *14*, 1437.
[29] N. Huebsch, P. R. Arany, A. S. Mao, D. Shvartsman, O. A. Ali, S. A. Bencherif, J. Rivera-Feliciano, D. J. Mooney, *Nat. Mater.* **2010**, *9*, 518.
[30] Y. Lei, S. Gojgini, J. Lam, T. Segura, *Biomaterials* **2011**, *32*, 39.
[31] M. Mehta, C. M. Madl, S. Lee, G. N. Duda, D. J. Mooney, *J. Biomed. Mater. Res., Part A* **2015**, *103*, 3516.
[32] M. R. Morgan, A. Byron, M. J. Humphries, M. D. Bass, *IUBMB Life* **2009**, *61*, 731.
[33] J. P. Kim, K. Zhang, J. D. Chen, R. H. Kramer, D. T. Woodley, *J. Biol. Chem.* **1994**, *269*, 26926.
[34] I. Schvartz, D. Seger, S. Shaltiel, *Int. J. Biochem. Cell Biol.* **1999**, *31*, 539.
[35] S. R. Braam, L. Zeinstra, S. Litjens, D. Ward-van Oostwaard, S. van den Brink, L. van Laake, F. Lebrin, P. Kats, R. Hochstenbach, R. Passier, A. Sonnenberg, C. L. Mummery, *Stem Cells* **2008**, *26*, 2257.
[36] T. J. Rowland, L. M. Miller, A. J. Blaschke, E. L. Doss, A. J. Bonham, S. T. Hikita, L. V. Johnson, D. O. Clegg, *Stem Cells Dev.* **2010**, *19*, 1231.
[37] D. H. Kim, D. Wirtz, *FASEB J.* **2013**, *27*, 1351.
[38] B. G. Keselowsky, D. M. Collard, A. J. García, *J. Biomed. Mater. Res., Part A* **2003**, *66A*, 247.
[39] K. Watanabe, M. Ueno, D. Kamiya, A. Nishiyama, M. Matsumura, T. Wataya, J. B. Takahashi, S. Nishikawa, S. Nishikawa, K. Muguruma, Y. Sasai, *Nat. Biotechnol.* **2007**, *25*, 681.
[40] S. K. Seidlits, C. T. Drinnan, R. R. Petersen, J. B. Shear, L. J. Suggs, C. E. Schmidt. *Acta Biomater.* **2011**, *7*, 2401.